CrossMark

ORIGINAL PAPER

The induction of apoptosis in SGC-7901 cells through the ROS-mediated mitochondrial dysfunction pathway by a Ir(III) complex

Cheng Zhang[1] · Shang-Hai Lai[1] · Chuan-Chuan Zeng[1] · Bing Tang[1] · Dan Wan[1] ·
De-Gang Xing[3] · Yun-Jun Liu[1,2]

Abstract A new ligand BTCP and its iridium(III) complex [Ir(ppy)$_2$(BTCP)]PF$_6$ (**Ir-1**) were synthesized and characterized by elemental analysis, ESI–MS, IR, ^{1}H NMR and ^{13}C NMR. The cytotoxic activity in vitro of the ligand and its complex against SGC-7901, HeLa, HOS, PC-12, BEL-7402, MG-63, SiHa, A549, HepG2 and normal cell LO2 were evaluated by MTT method [MTT = (3-(4,5-dimethyl-thiazol-2-yl)-2,5-diphenyltetrazolium bromide)]. The apoptosis was assayed with AO/EB and Hoechst 33258 staining methods. The reactive oxygen species (ROS), mitochondrial membrane potential, autophagy and cell invasion were studied under fluorescent microscope. The expression of caspases and Bcl-2 family proteins were investigated by western blot. The IC$_{50}$ values of complex toward SGC-7901, BEL-7402 and MG-63 cells are 3.9 ± 0.5, 5.4 ± 1.2 and 4.2 ± 0.6 μM. The complex can increase the levels of ROS, and induce a decrease in the mitochondrial membrane potential. **Ir-1** inhibits the cell growth at G0/G1 phase in SGC-7901 cells, and the complex can induce both autophagy and apoptosis and inhibit the cell invasion. And the complex induces apoptosis through a ROS-mediated mitochondrial dysfunction pathway.

Keywords Ir(III) complex · Apoptosis · Autophagy · Cell invasion · Bcl-2 family proteins

✉ De-Gang Xing
  degangxing@126.com

✉ Yun-Jun Liu
  lyjche@163.com

1 School of Pharmacy, Guangdong Pharmaceutical University, Guangzhou 510006, People's Republic of China

2 Guangdong Cosmetics Engineering and Technology Research Center, Guangzhou 510006, People's Republic of China

3 School of Basic Science, Guangdong Pharmaceutical University, Guangzhou 510006, People's Republic of China

Introduction

Due to the uncontrolled cell proliferation, invasion of surrounding and distant tissues aggressive metastasis [1], cancer is generally considered as a group of complex and multifaceted diseases [2]. Since the clinical success of cisplatin, transition metal platinum drugs such as oxaliplatin, cisplatin and carboplatin have been effectively utilized in treating amount of cancer disease [3]. Accompanied with the severe side effects of platinum-based drugs, a number of research groups try to develop anti-proliferative properties of metal complexes other than platinum [4–8]. As the rapid development of anticancer drugs, the therapeutic value of metal-based drugs, such as ruthenium [9], osmium [10], rhenium [11], as well as others, have long been established [12]. On the contrast, the studies on anticancer activity of iridium complexes have been paid less attention. However, in the recent years, organometallic ligands iridium complexes are taken as an alternative to platinum-based drugs owing to their higher antineoplastic activity, less side effects, and photochemical activity and redox properties [13–15]. As anticancer drugs, some of Ir(III) complexes containing various peripheral ligands such as half-sandwich [16–18], CO [19], carbine [20], metallocenes [21], were designed to implement their cytotoxicity through DNA, enzyme, or cytoplasmic-based mechanisms. Chao and co-worker synthesized a series of polypyridyl

iridium compounds, which exhibited high cytotoxic effects on cancer cells [22]. Meanwhile, mitochondria as the main target of cyclometalated iridium(III) complexes have been proved [23–26]. As one of the major cell regulated centers, the important function of mitochondria lies in that the mitochondria control the energy production in the living cell and involved in many other cellular activities [27, 28]. To obtain more insight into the anticancer and further understanding the anticancer mechanism of iridium complex, in this article, a new cyclometalated iridium(III) complex [Ir(ppy)$_2$(BTCP)]PF$_6$ [ppy = 2-phenylpyridine, BTCP = 2-bicyclo[2.2.1]hept-5-en-yl-1H-1,3,7,8-tetraazacyclopenta[l]phenanthrene, **Ir-1**, Scheme 1] was designed and synthesized. The cytotoxicity in vitro was evaluated by MTT method. The apoptosis, cellular uptake, reactive oxygen species, mitochondrial membrane potential, cell cycle arrest, autophagy, cell invasion and expression of Bcl-2 family proteins were studied in detail. The complex can induce autophagy and apoptosis through a ROS-mediated mitochondrial dysfunction pathway.

Materials and methods

All reagents and solvents were purchased commercially and used without further purification unless otherwise noted. Ultrapure MilliQ water was used in all experiments. DMSO, 5-norbornene-2-carboxaldehyde and RPMI 1640 were purchased from Sigma. 1,10-phenanthroline was obtained from the Guangzhou Chemical Reagent Factory. Cancer cell lines of SGC-7901 (human gastric adenocarcinoma), HeLa (human cervical cancer), HOS (human osteosarcoma), PC-12 (pheochromocytoma), BEL-7402 (human hepatocellular carcinoma), MG-63 (human osteosarcoma), SiHa (human cervical carcinone), A549 (human lung carcinoma), HepG2 (human hepatocellular carcinoma) and normal cell LO2 (human liver cell) were purchased from the American Type Culture Collection. IrCl$_3$·3H$_2$O was purchased from the Kunming Institution of Precious Metals.

Microanalysis (C, H, and N) was carried out with a Perkin-Elmer 240Q elemental analyzer. Electrospray ionization mass spectra (ESI–MS) were recorded on a LCQ system (Finnigan MAT, USA) using acetonitrile as mobile phase. The spray voltage, tube lens offset, capillary voltage and capillary temperature were set at 4.50 kV, 30.00 V, 23.00 V and 200 °C, respectively, and the quoted m/z values are for the major peaks in the isotope distribution. ^{1}H NMR and ^{13}C NMR spectra were recorded on a Varian-500 spectrometer with DMSO-d$_6$ as solvent and tetramethylsilane (TMS) as an internal standard at 500 MHz at room temperature.

Synthesis of ligand BTCP

1,10-phenanthroline-5,6-dione (0.315 g, 1.5 mmol) [29], 5-norbornene-2-carboxaldehyde (0.183 g, 1.5 mmol), ammonium acetate (2.31 g, 30 mmol), and glacial acetic acid (20 cm^3) was refluxed with stirring for 2 h. The cooled solution was diluted with water and neutralized with concentrated aqueous ammonia. The brown precipitate was collected and purified by column chromatography on silica gel (60–100 mesh) with ethanol as eluent to give the compound as a brown powder. Yield: 83%. Anal. Calcd for C$_{20}$H$_{16}$N$_4$: C, 76.90; H, 5.16; N, 17.94. Found: C, 76.70; H, 5.31; N, 17.86%. IR (KBr, cm^{-1}): 2964.9, 1620.4, 1431.8, 1355.5, 1179.9, 1131.6, 1071.8, 1025.1, 807.8, 741.3, 720.6, 626.2. FAB-MS: $m/z = 313$ [M + 1].

Synthesis of complex [Ir(ppy)$_2$(BTCP)]PF$_6$ (Ir-1)

A mixture of cis-[Ir(ppy)$_2$Cl$_2$]$_2$ [30] (0.15 g, 0.14 mmol) and BTCP (0.087 g, 0.28 mmol) in a mixture of 15 mL chloroform and methanol (V$_{CHCl_3}$:V$_{CH_3COCH_3}$ = 2:1) was refluxed under argon for 5 h to give a clear yellow solution. Upon cooling, a yellow precipitate was obtained by dropwise addition of saturated aqueous NH$_4$PF$_6$ solution with stirring at room temperature for 2 h. The crude product was purified by column chromatography on neutral alumina with a mixture of CH$_2$Cl$_2$–acetone (1:3, v/v) as eluent.
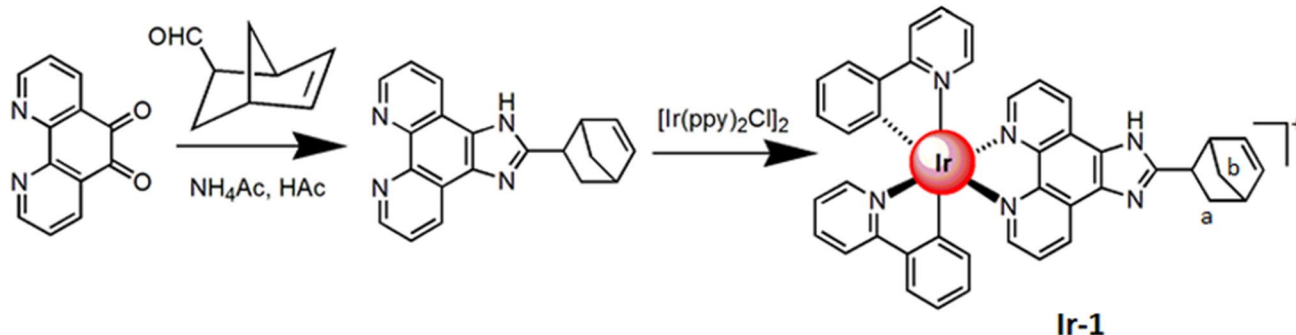
Scheme 1 The synthetic route of ligand and its complex **Ir-1**

The yellow band was collected. The solvent was removed under reduced pressure and a yellow powder was obtained. Yield: 70%. Anal. Calc for $C_{42}H_{32}N_6IrPF_6$: C, 52.60; H, 3.37; N, 8.77%. Found: C, 52.46; H, 3.48; N, 8.68%. IR (KBr, cm^{-1}): 3381.5, 3060.7, 2970.9, 1693.6, 1607.0, 1583.3, 1548.1, 1478.7, 1439.1, 1420.5, 1365.2, 1306.5, 1164.5, 759.6, 557.8. ^1H NMR (DMSO-d_6): δ 13.94 (s, 1H), 9.10 (d, 2H, $J = 8.0$ Hz), 8.25 (d, 2H, $J = 8.0$ Hz), 8.12 (d, 2H, $J = 6.0$ Hz), 8.04 (d, 2H, $J = 5.0$ Hz), 7.95 (d, 2H, $J = 8.0$ Hz), 7.86 (t, 2H, $J = 8.0$ Hz), 7,47 (t, 2H, $J = 5.5$ Hz), 7.05 (t, 2H, $J = 7.5$ Hz), 6.96 (d, 2H, $J = 6.0$ Hz), 6.28 (d, 4H, $J = 6.5$ Hz), 5.80 (d, 1H, $J = 5.5$ Hz), 5.77 (d, 1H, $J = 5.5$ Hz), 3.80 (t, 1H, $J = 5.0$ Hz), 3.54 (t, 1H, $J = 4.5$ Hz), 2.55 (s, 2H), 2.04 (d, 1H, $J = 1.0$ Hz), 1.84 (d, 2H, $J = 5.5$ Hz). ^{13}C NMR: (DMSO-d_6, 125 MHz, ppm): 166.8, 149.1, 144.0, 138.6, 132.7, 131.2, 130.2, 125.0, 123.8, 122.3, 119.9, 68.7, 68.5, 56.7, 55.8, 46.8, 40.0, 32.1, 29.6, 29.5. ESI–MS (CH_3CN): m/z 813.2 ($[M-PF_6]^+$). The stability of the complex was investigated by UV–Vis spectra. The complex was dissolved in a minimum amount of DMSO (0.5% of the final volume) and then diluted with PBS to a required concentration. As shown in Fig. S1 (supporting information), no obvious changes in absorbance are observed at 0 and 24 h. The luminescence spectra of the complex is shown in Fig. S2 (supporting information), the complex can emit luminescence in PBS solution at ambient temperature, with a maximum appearing at 561 nm, and the luminescence intensity increases with increasing the concentration of **Ir-1**.

Cytotoxic activity evaluation in vitro

3-(4,5-Dimethylthiazole)-2,5-diphenyltetrazolium bromide (MTT) assay procedures were used [31]. Cells were placed in 96-well microassay culture plates (8×10^3 cells per well) and grown overnight at 37 °C in a 5% CO_2 incubator. The tested complexes were dissolved in DMSO and then added to the wells to achieve final concentrations ranging from 10^{-6} to 10^{-4} M. Control wells were prepared by addition of culture medium (100 μL). The plates were incubated at 37 °C in a 5% CO_2 incubator for 48 h. Upon completion of the incubation, stock MTT dye solution (20 μL, 5 mg/mL^{-1}) was added to each well. After 4 h, buffer (100 μL) containing dimethylformamide (50%) and sodium dodecyl sulfate (20%) was added to solubilize the MTT formazan. The optical density of each well was measured with a microplate spectrophotometer at a wavelength of 490 nm. The IC_{50} values were determined by the percentage of cell viability versus concentration on a logarithmic graph and reading off the concentration at which 50% of cells remain viable relative to the control. Each experiment was repeated at least three times to obtain the mean values.

Apoptosis assay by AO/EB and Hoechst 33258 staining methods

SGC-7901 cells were seeded onto chamber slides in six-well plates at a density of 2×10^5 cells per well and incubated for 24 h. The cells were cultured in RPMI (Roswell Park Memorial Institute) 1640 supplemented with 10% of fetal bovine serum (FBS) and incubated at 37 °C in 5% CO_2. The medium was removed and replaced with medium (final DMSO concentration, 0.05% v/v) containing the complex (3.13 and 6.25 μM) for 24 h. The medium was removed again, and the cells were washed with ice-cold phosphate buffer saline (PBS), and fixed with formalin (4%, w/v). Cell nuclei were counterstained with acridine orange (AO) and ethidium bromide (EB) (AO: 100 μg/mL, EB: 100 μg/mL) or Hoechst 33258 for 10 min. The cells were observed and imaged under a fluorescence microscope (Nikon, Yokohama, Japan) with excitation at 350 nm and emission at 460 nm.

DNA damage assay

DNA damage was investigated by means of comet assay. BEL-7402 cells in culture medium were incubated with 3.13 and 6.25 μM of complex for 24 h at 37 °C. The cells were harvested by a trypsinization process at 24 h. A total of 100 μL of 0.5% normal agarose in PBS was dropped gently onto a fully frosted microslide, covered immediately with a coverslip, and then placed at 4 °C for 10 min. The coverslip was removed after the gel had been set. A mixture of 50 μL of the cell suspension (200 cells/μL) mixed with 50 μL of 1% low melting agarose was preserved at 37 °C. A total of 100 μL of this mixture was applied quickly on top of the gel, coated over the microslide, covered immediately with a coverslip, and then placed at 4 °C for 10 min. The coverslip was again removed after the gel had been set. A third coating of 50 μL of 0.5% low melting agarose was placed on the gel and allowed to place at 4 °C for 15 min. After solidification of the agarose, the coverslips were removed, and the slides were immersed in an ice-cold lysis solution (2.5 M NaCl, 100 mM EDTA, 10 mM Tris, 90 mM sodium sarcosinate, NaOH, pH 10, 1% Triton X-100 and 10% DMSO) and placed in a refrigerator at 4 °C for 2 h. All of the above operations were performed under low lighting conditions to avoid additional DNA damage. The slides, after removal from the lysis solution, were placed horizontally in an electrophoresis chamber. The reservoirs were filled with an electrophoresis buffer (300 mM NaOH, 1.2 mM EDTA) until the slides were just immersed in it, and the DNA was allowed to unwind for 30 min in electrophoresis solution. Then the electrophoresis was carried out at 25 V and 300 mA for 20 min. After electrophoresis, the slides were removed, washed thrice in a neutralization

buffer (400 mM Tris, HCl, pH 7.5). Cells were stained with 20 μL of EB (20 μg·mL^{-1}) in the dark for 20 min. The slides were washed in chilled distilled water for 10 min to neutralize the excess alkali, air-dried and scored for comets by fluorescent microscopy.

Cellular uptake

SGC-7901 cells were placed in 24-well microassay culture plates (4×10^4 cells per well) and grown overnight at 37 °C in a 5% CO_2 incubator. Different concentrations of **Ir-1** were then added to the wells. The plates were incubated at 37 °C in a 5% CO_2 incubator for 24 h. Upon completion of the incubation, the wells were washed three times with PBS. After discarding the culture medium, the cells were visualized by fluorescent microscopy.

Reactive oxygen species (ROS) detection

SGC-7901 cells were seeded into six-well plates (Costar, Corning Corp, New York, USA) at a density of 2×10^5 cells per well and incubated for 24 h. The cells were cultured in RPMI 1640 supplemented with 10% of FBS and incubated at 37 °C in 5% CO_2. The medium was removed and replaced with medium (final DMSO concentration, 0.05% v/v) containing different concentration of complex for 24 h. The medium was removed again. The fluorescent dye 2′,7′-dichlorodihydrofluorescein diacetate (DCHF-DA, 10 μM) was added to the medium to cover the cells. The treated cells were then washed with cold PBS-EDTA twice, collected by trypsinization and centrifugation at 1500 rpm for 5 min, the cell pellets were suspended in PBS-EDTA and imaged under a fluorescent microscope. The DCF fluorescent intensity was determined by flow cytometry.

Mitochondrial membrane potential assay

SGC-7901 cells were treated for 24 h with different concentration of the complex in 12-well plates and were then washed three times with cold PBS. The cells were detached with trypsin–EDTA solution. Collected cells were incubated for 20 min with 1 μg/mL of JC-1 (5,5′,6,6′-tetrachloro-1,1′,3,3′-tetraethyl-imidacarbocyanine iodide) in culture medium at 37 °C in the dark. Cells were immediately centrifuged to remove the supernatant. Cell pellets were suspended in PBS and imaged under fluorescence microscope. The ratio of red/green fluorescence intensity was determined by flow cytometry.

Cell cycle arrest by flow cytometry

SGC-7901 cells were seeded into six-well plates (Costar, Corning Corp, New York, USA) at a density of 2×10^5

cells per well and incubated for 24 h. The cells were cultured in RPMI 1640 supplemented with 10% of FBS and incubated at 37 °C in 5% CO_2. The medium was removed and replaced with medium (final DMSO concentration, 0.05% v/v) containing complex (6.25 μM). After incubation for 24 h, the cell layer was trypsinized and washed with cold PBS and fixed with 70% ethanol. Twenty microliters of RNAse (0.2 mg/mL) and 20 μL of propidium iodide (0.02 mg/mL) were added to the cell suspensions and they were incubated at 37 °C for 30 min. Then the samples were analyzed with a FACSCalibur flow cytometry. The number of cells analyzed for each sample was 10,000 [32].

Autophagy induced by complex

SGC-7901 cells were seeded onto chamber slides in 12-well plates and incubated for 24 h. The cells were cultured in RPMI 1640 supplemented with 10% of FBS and incubated at 37 °C in 5% CO_2. The medium was removed and replaced with medium (final DMSO concentration, 0.05% v/v) containing different concentration of complex for 24 h. The medium was removed again, and the cells were washed with ice-cold PBS twice. Then the cells were stained with MDC (monodansylcadaverine) solution (50 μM) for 10 min and washed with PBS twice. The cells were observed and imaged under fluorescence microscope. The effect of the complexes on the expression of LC3 protein was assayed by western blot.

The effect of autophagy on cell viability

Cell viability was studied using the MTT method. Cells were placed in 96-well microassay culture plates (8×10^4 cells per well) and cultured overnight at 37 °C in a 5% CO_2 incubator. The cells were pretreated with or without 3-methyladenine (3-MA, 3 mM) for 3 h, followed by different concentration of **Ir-1** for 24 h. After incubation, cells were incubated with MTT (0.5 mg/ml) for 4 h at 37 °C. Upon completion of the incubation, 100 μL DMSO was added to solubilize the MTT formazan. The optical density of each well was then measured with a microplate spectrophotometer at a wavelength of 490 nm. The viability (%) of cell growth was calculated by the formula: $(A_{490 \text{ (treatment group)}}/A_{490 \text{ (control)}}) \times 100$, $A_{490 \text{ (treatment group)}}$ is the mean OD value of cells treated with the various ruthenium complexes and $A_{490 \text{ (control)}}$ is the mean OD value of untreated cells. Each experiment was repeated at least three times to obtain the mean values.

Matrigel invasion assay

The BD Matrigel invasion chamber was used to investigate the cell invasion according to the manufacturer's instructions. SGC-7901 cells (4×10^4) in serum free media and

different concentration of the complex were seeded in the top chamber of the two chamber Matrigel system. RPMI-1640 (20% FBS) was added as chemo-attractant into the lower chamber. Cells were allowed to invade for 24 h. After incubation, non-invading cells were removed from the upper surface and cells on the lower surface were fixed with 4% paraformaldehyde and stained with 0.1% of crystal violet. The membranes were photographed and the invading cells were counted under a light microscope. The mean values from three independent assays were calculated.

The expression of caspases and Bcl-2 family proteins

SGC-7901 cells were seeded in 3.5 cm dishes for 24 h and incubated with 3.13 and 6.25 µM of the complex in the presence of 10% FBS. The cells were harvested in lysis buffer. After sonication, the samples were centrifuged for 20 min at 13,000g. The protein concentration of the supernatant was determined by BCA (bicinchoninic acid) assay. Sodium dodecyl sulfate–polyacrylamide gel electrophoresis was done loading equal amount of proteins per lane. Gels were then transferred to poly (vinylidene difluoride) membranes (Millipore) and blocked with 5% non-fat milk in TBST (20 mM Tris–HCl, 150 mM NaCl, 0.05% Tween 20, pH 8.0) buffer for 1 h. Then the membranes were incubated with primary antibodies at 1:5000 dilutions in 5% non-fat milk overnight at 4 °C, and washed four times with TBST for a total of 30 min. After which the secondary antibodies conjugated with horseradish peroxidase at 1:5000 dilution for 1 h at room temperature and then washed four times with TBST. The blots were visualized with the Amersham ECL Plus western blotting detection reagents according to the manufacturer's instructions. To assess the presence of comparable amount of proteins in each lane, the membranes were stripped finally to detect the β-actin. The gray values were calculated with BandScan.

Results and discussion

Synthesis and characterization

The ligand BTCP was prepared by the reaction of 1,10-phenanthroline-5,6-dione and 5-norbornene-2-carboxaldehyde in the presence of ammonium acetate and glacial acetic acid. The complex [Ir(ppy)$_2$(BTCP)]PF$_6$ (**Ir-1**) was synthesized by the direct reaction of BTCP and precursor complex cis-[Ir(ppy)$_2$Cl$_2$]$_2$ in a mixture of chloroform and methanol. The ligand and **Ir-1** were characterized by elemental analysis, IR, ESI–MS and NMR. In the ESI–MS spectra for the complex, the expected signal [M-PF$_6$]$^+$ was observed. The measured molecular weight was consistent with the expected value. In the assay of IR spectra, 2964.9 cm^{-1} for BCTP and 2970.9 cm^{-1} for **Ir-1** are assigned to C–H stretch vibration. 3381.5 cm^{-1} for **Ir-1** is attributed to N–H stretch vibration. In the ^{13}C NMR spectra, 29.6 and 29.5 ppm are attributed to C_a and C_b, respectively.

Cytotoxic activity in vitro

The in vitro cytotoxicity of the tested complex is a usual concern in anticancer drug study. The cytotoxicity of ligand and complex **Ir-1** against SGC-7901, HOS, PC-12, HeLa, BEL-7402, SiHa, MG-63, HepG-2, A549 and normal cell LO2 was assayed using MTT method after 48 h of incubation and cisplatin was used as positive control, the IC$_{50}$ values are listed in Table 1, As expectation, ligand BTCP has no cytotoxicity against the selected cell lines, whereas **Ir-1** complex displays different cytotoxic activity towards different cancer cell lines. Particularly, **Ir-1** shows high inhibition of cell growth in SGC-7901, MG-63 and SiHa cell with a low IC$_{50}$ value of 3.9 ± 0.6, 5.4 ± 1.2 and 4.1 ± 0.6 µM, respectively. Interestingly, **Ir-1** exhibits higher cytotoxic effect than cisplatin on PC-12, BEL-7402, MG-63 and SiHa cells under identical conditions. Unfortunately, the complex also reveals a certain extent cytotoxicity against normal cell LO2 (IC$_{50}$ = 10.4 ± 1.5 µM). Comparing the cytotoxicity of **Ir-1** with other Ir(III) complexes, the cytotoxic activity of **Ir-1** is lower than those of iridium β-carboline complexes (IC$_{50}$ = 1.6 ± 0.2 µM) against A549 cell [33] and Ir(pq)$_2$(bpy-CONH-Et)]PF$_6$ (IC$_{50}$ = 5.5 ± 0.4 µM against HeLa cell, pq = 2-phenylquinoline, bpy-CONH-Et = 4-(N-(2-(ω-methoxypoly-(1-oxapropyl))ethyl)aminocarbonyl)-4′-methyl-2,2′-bipyridine) [34]. Because SGC-7901 cell is sensitive to the complex, this cell line was selected to undergo the following experiments.

Table 1 IC$_{50}$ values of BTCP and complexes [Ir(ppy)$_2$Cl$_2$]$_2$, **Ir-1** toward the selected cell lines

comp	SGC-7901	HeLa	HOS	PC-12	BEL-7402	MG-63	SiHa	A549	HepG2	LO2
BTCP	>200	>200	>200	>200	>200	>200	>200	>200	>200	>200
[Ir(ppy)$_2$Cl$_2$]$_2$	32.8 ± 3.3	37.3 ± 2.5	–	–	30.1 ± 2.2	–	–	–	–	–
Ir-1	3.9 ± 0.5	13.9 ± 2.3	6.0 ± 1.1	5.7 ± 1.1	5.4 ± 1.2	4.2 ± 0.8	4.1 ± 0.6	9.6 ± 2.3	12.7 ± 1.8	10.4 ± 1.5
Cisplatin	3.6 ± 0.5	7.0 ± 1.0	2.6 ± 0.3	11.2 ± 0.7	10.8 ± 1.6	6.6 ± 0.5	13.6 ± 2.2	7.5 ± 1.3	12.5 ± 1.5	9.2 ± 1.4

Apoptosis assay by AO/EB and Hoechst 33258 staining methods

Morphological analyses is one of the considerations in process of apoptosis, most of the cytotoxic antitumor drugs in current use have been shown to induce apoptosis in susceptible cells [35]. To determine whether **Ir-1** induce cell death by apoptosis, the AO/EB straining assay was performed. After treatment of SGC-7901 cells with **Ir-1** for 24 h, the images of the cells stained with AO/EB are shown in Fig. 1. In the control (a), the living cells keep integrated morphology with bright green in spots. However, SGC-7901 cells exposure to 3.13 (b) and 6.25 μM (c) of **Ir-1**, with increasing the concentration of **Ir-1**, more apoptotic cells exhibited apoptotic characteristic such as nuclear shrinkage and chromatin condensation were found. The apoptosis was also assayed with Hoechst 33258 staining method (d–f), the apoptotic features were also observed. The observations indicated that the complex can induce apoptosis in SGC-7901 cells. To further quantitatively compare the effect of the complex concentration on the apoptosis, the percentage in the apoptotic cells was determined using double staining of Annexin V and PI [36] by flow cytometry. As shown in Fig. 2, in the control (a), the percentages of apoptotic and necrotic cells are 0.00 and 0.04%. Comparing to the control, the percentages of apoptotic and necrotic cells treated with 3.13 (b) and 6.25 μM (c) of **Ir-1** are 2.54% and 3.15, 13.38 and 2.89%, respectively. The results suggest that **Ir-1** induces apoptosis in SGC-7901 cell in dose-dependent manner.

Cellular uptake assay

Cellular uptake is the first step to the success of anticancer drugs. In this study, the cellular uptake properties of the complex have been investigated using fluorescent microscope. The images of SGC-7901 cells treated with 3.13 μM of **Ir-1** for 24 h and the cells were strained with

Fig. 1 Apoptosis in SGC-7901 cell (**a**, **d**) treated by 3.13 (**b**, **e**) and 6.25 (**c**, **f**) μM of **Ir-1** for 24 h and the cells were stained with AO/EB (**a–c**) and Hoechst 33258 (**d–f**)
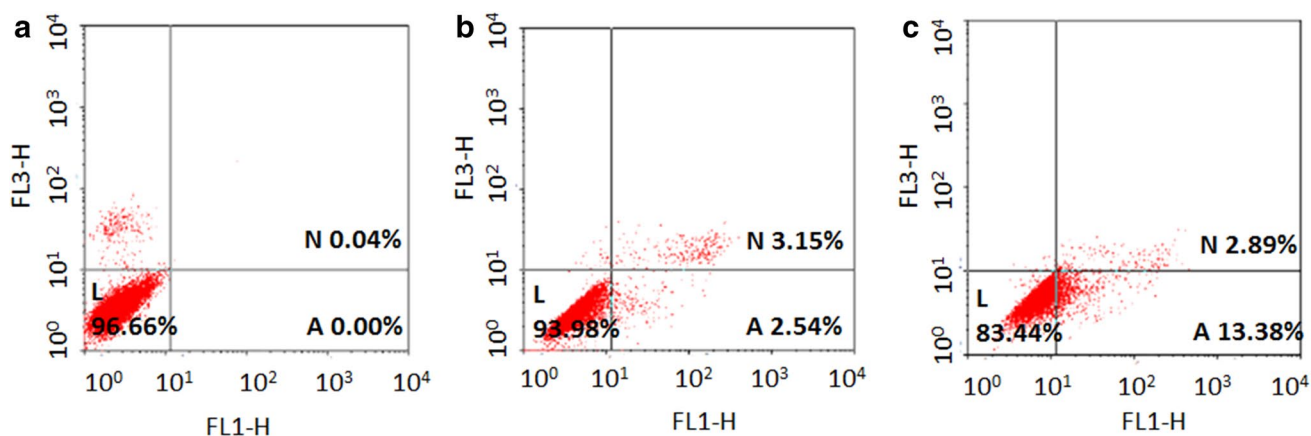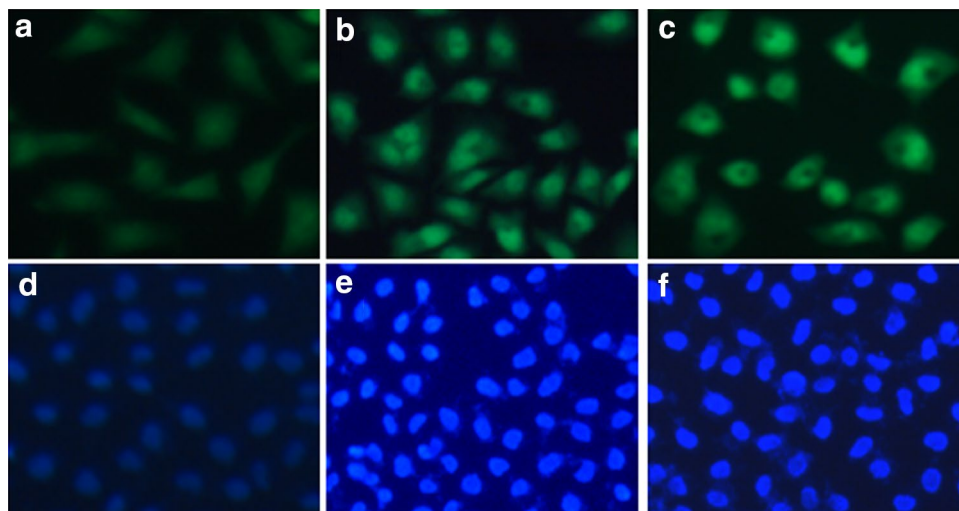

Fig. 2 The percentage of living (L), necrotic (N) and apoptotic (A) cells was assayed by flow cytometry after SGC-7901 cell (**a**) was treated with 3.13 (**b**) and 6.25 (**c**) μM of **Ir-1** for 24 h

DAPI (4′,6-diamidino-2-phenylindole) dye, and the cells were observed under a fluorescent microscope. As shown in Fig. 3A, DAPI staining located the nucleus emits blue luminescence with excitement at 340 nm. **Ir-1** emits green fluorescence with an excitation wavelength at 350 nm, and the merged picture was obtained from the DAPI and **Ir-1** emission. The merge manifests cellular association of the complex. The results show that the complex **Ir-1** can enter into the cytoplasm and accumulate in the cell nuclei. To further confirm the phenomenon and the effect of the concentration of the complex on cellular uptake, the cellular uptake was also investigated by flow cytometry. As shown in Fig. 3B, in the control (a), the emission intensity is 5.84. After SGC-7901 cells were treated with 3.13 (b), 6.25 (c) and 12.5 (d) μM of **Ir-1**, the emission intensity is 44.1, 90.4 and 233. Obviously, more **Ir-1** was uptaken by SGC-7901 cells with increasing the concentration of

Ir-1. The results show that complex **Ir-1** can be uptaken and the uptake effect displays a concentration-dependent manner.

DNA damage studies

Comet assay provide an image of the changes that have happened in the chromatin organization in a single cell, which is regarded as a more effective and simple way to detect DNA fragmentation or DNA damage in a cell population [37]. When a cell with damaged DNA is subjected to electrophoresis and then stained with EB, it appears as a comet [38]. SGC-7901 cells were incubated with 3.13 and 6.25 μM of **Ir-1** for 24 h. As shown in Fig. 4, in the control (a), SGC-7901 cells fail to show a comet like appearance. On the contrary, the nuclei of the treated cells appeared well-formed comets, and the length of the

Fig. 3 A Images of SGC-7901 cell exposure to 3.13 (*a*) and 6.25 μM (*b*) of **Ir-1** for 24 h and stained with DAPI. **B** The fluorescent intensity of SGC-7901 (*a*) treated with 3.13 (*b*), 6.25 (*c*) and 12.5 (*d*) μM of **Ir-1** for 24 h was determined by flow cytometry
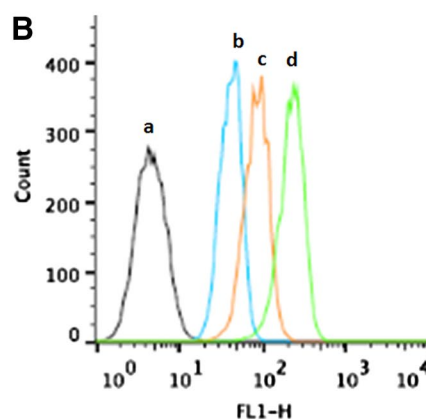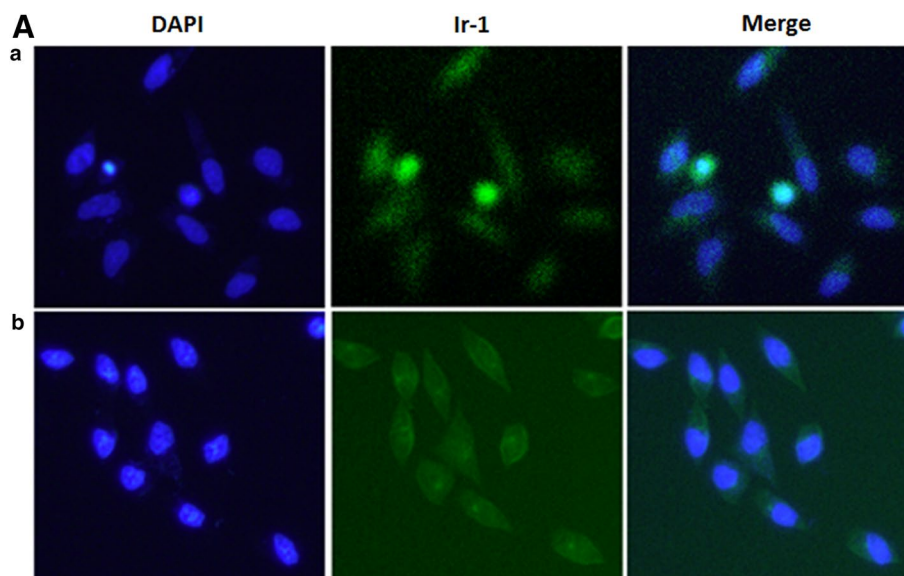
Fig. 4 Comet assay of EB-stained SGC-7901 cell (**a**) exposure to 3.13 (**b**) and 6.25 (**c**) µM of **Ir-1** for 24 h
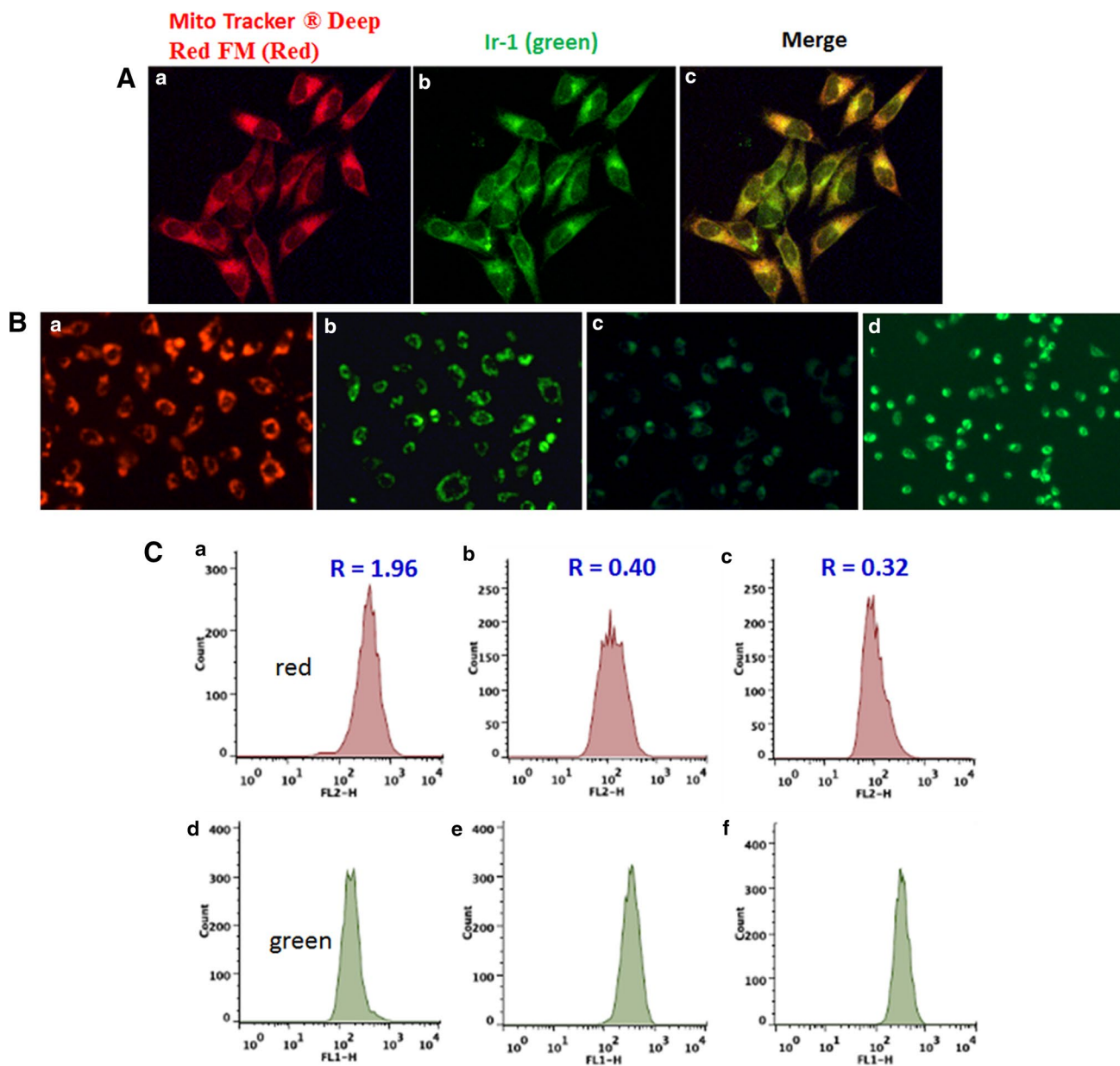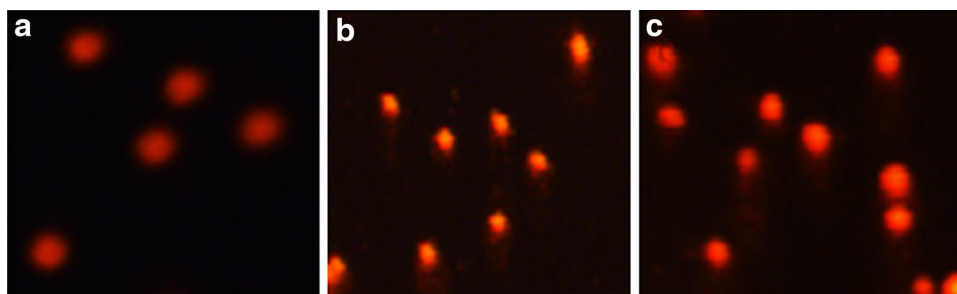

Fig. 5 A The localization of **Ir-1** in the mitochondria. SGC-7901 (*a*) was exposed to 3.13 µM of **Ir-1** (*b*) for 1 h and the cells were stained with Mito Tracker® Deep Red FM and imaged under fluorescent microscope. **B** Assay of SGC-7901 cell mitochondrial membrane potential with JC-1 as fluorescent probe. SGC-7901 (*a*) exposure to cccp (*b*, positive control) and 3.13 (*c*) and 6.25 (*d*) µM of **Ir-1** for 24 h. **C** The ratio of red/green fluorescent intensity was determined by flow cytometry after SGC-7901 (*a*, *d*) was treated with 3.13 (*b*, *e*) and 6.25 (*c*, *f*) µM of **Ir-1** for 24 h
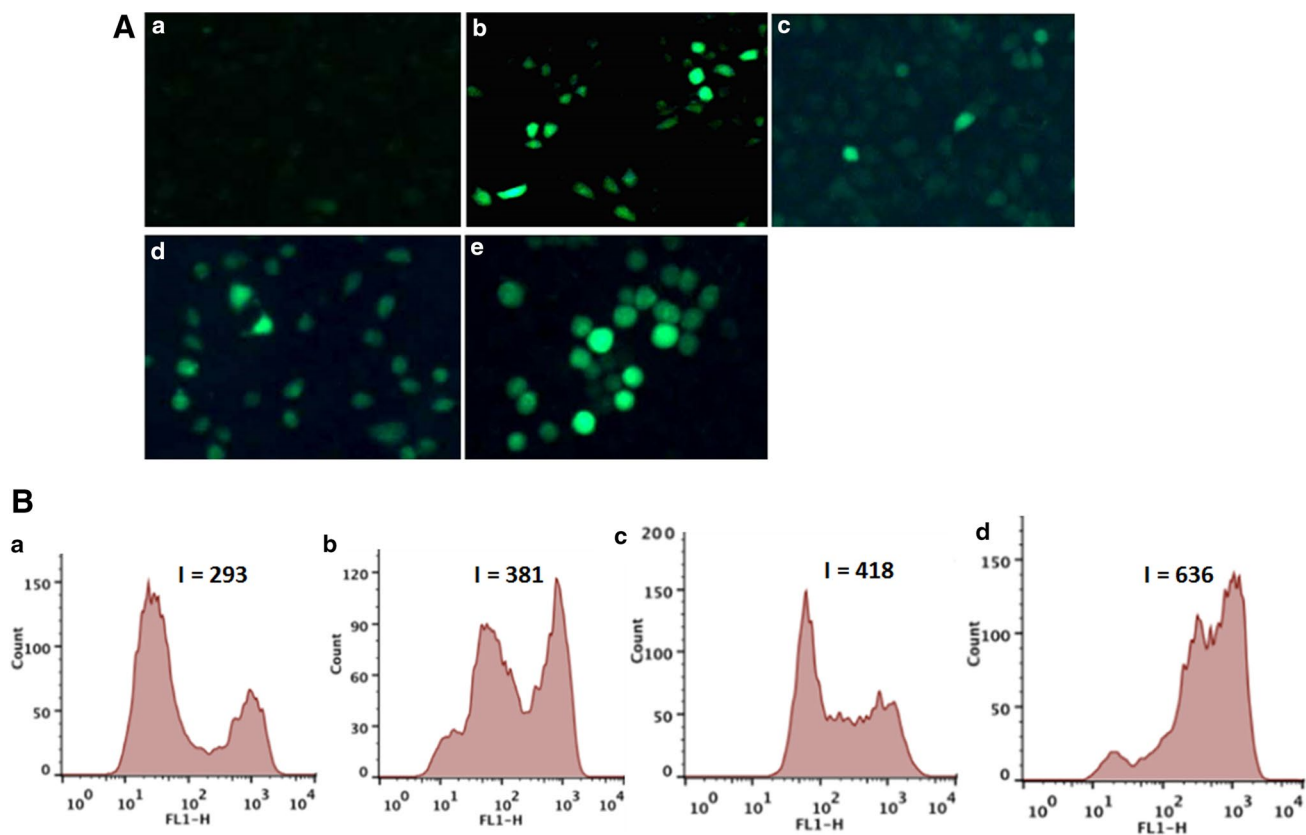
Fig. 6 A ROS generation in SGC-7901 cell (*a*) treated with Rosup (*b*, positive control) and 3.13 (*c*), 6.25 (*d*) and 12.5 (*e*) µM of **Ir-1** for 24 h. **B** DCF fluorescent intensity of SGC-7901 cell (*a*) exposure to 3.13 (*b*), 6.25 (*c*) and 12.5 (*d*) µM of **Ir-1** for 24 h was determined by flow cytometry
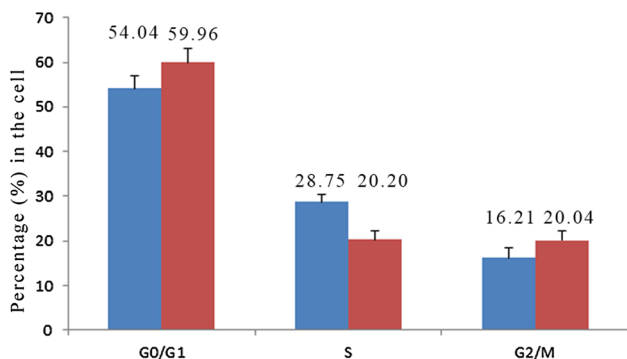

Fig. 7 The cell cycle arrest in SGC-7901 (*blue*) induced by 6.25 µM of **Ir-1** (*red*) for 24 h

comet tail, shown dose-dependent manner, revealed the extent of DNA strand breaks (b, c). The results manifest that the complex can induce DNA damage in SGC-7901 cells.

Assay of mitochondrial membrane potential (MMP)

Mitochondria play a key role in keeping genomic integrity by continuously oxidizing substrates and holding a proton gradient through the lipid bilayer with a great mitochondrial membrane potential [39]. To investigate the localization of the complex in the mitochondria, Mito Tracker® Deep Red FM (ThermoFisher, 100 nM) was used as red fluorescent probe. As shown in Fig. 5A, in the control (a), the mitochondria were stained in red. After the treatment of SGC-7901 cells with 3.13 µM of **Ir-1**, the complex emits green fluorescence (b). The merge (c) of the red and the green indicates that the complex can enter into the mitochondria. To further determine whether the apoptotic cells are accompanied by mitochondrial dysfunction, the changes of MMP are detected using a fluorescence microscope and flow cytometry after staining live cells with dye JC-1. JC-1 forms aggregate and emits red fluorescence signals corresponding to high mitochondrial membrane potential, on
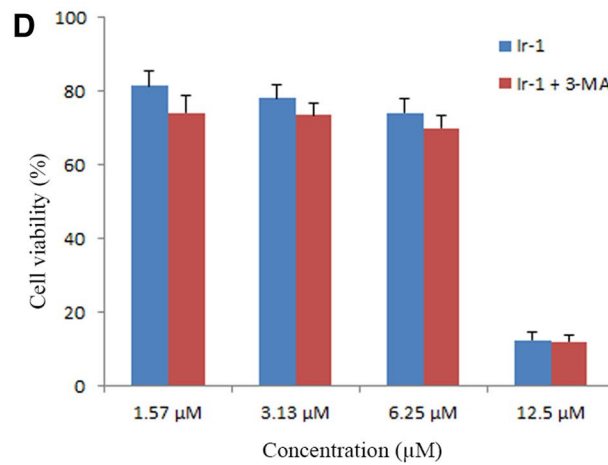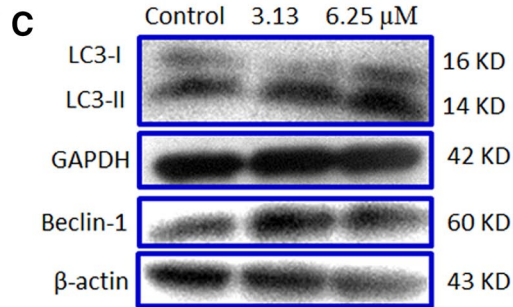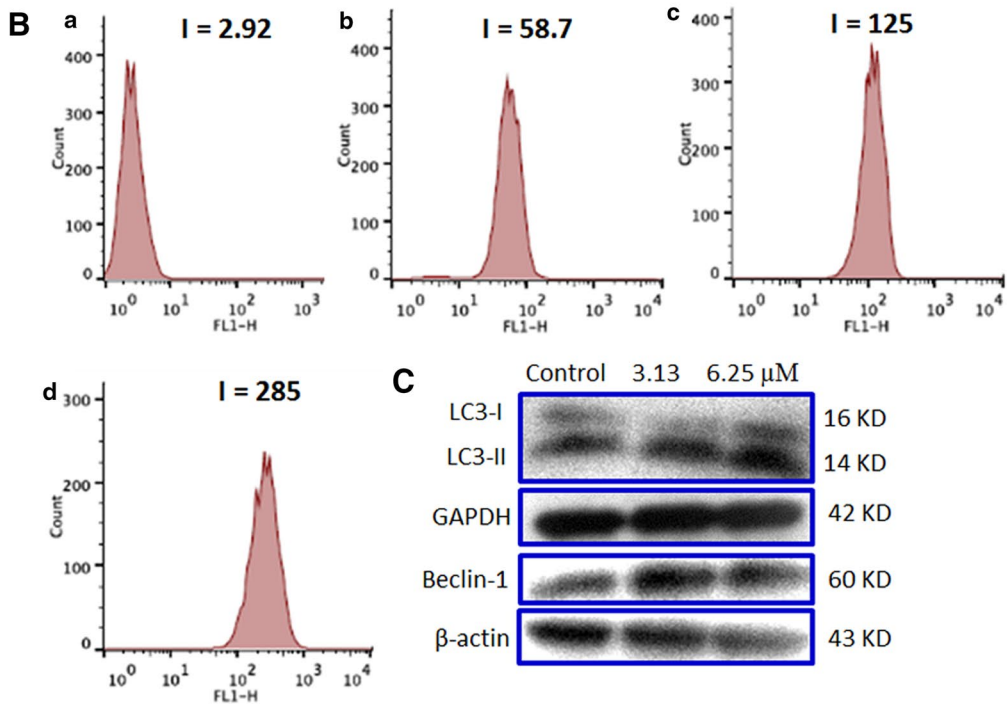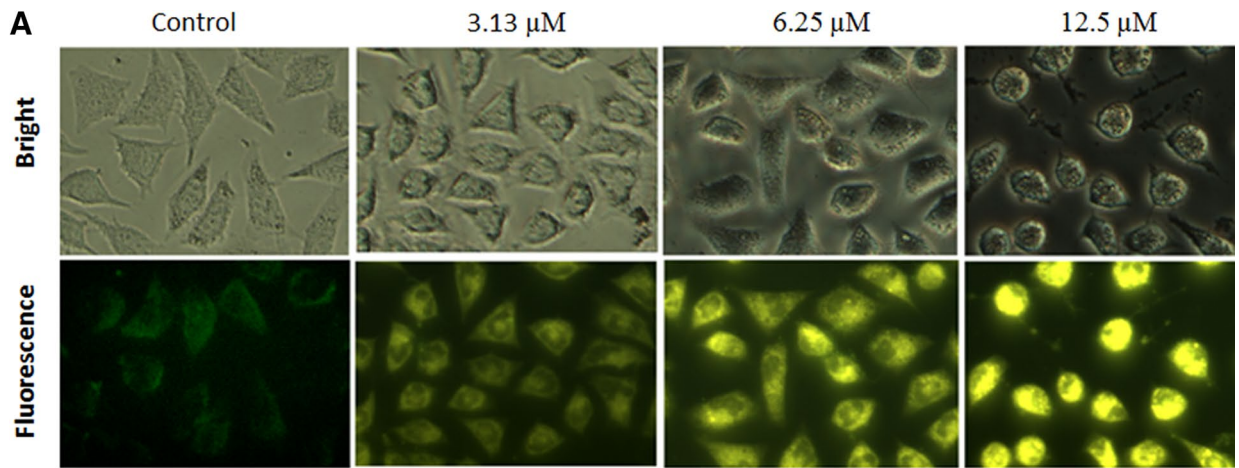
◀**Fig. 8** **A** Autophagy in SGC-7901 cells induced by different concentration of **Ir-1** for 24 h. Autophagy was detected using MDC staining. **B** The green fluorescent intensity (I) of SGC-7901 (*a*) exposure to 3.13 (*b*), 6.25 (*c*) and 12.5 (*d*) μM was determined by flow cytometry. **C** The protein levels of LC-3 and Beclin-1 were assayed by western blot analysis. GAPDH was used as internal control. **D** The effect of autophagy on the cell viability

the contrary, JC-1 exists as monomer and emits green fluorescence signals corresponding to low membrane potential [40]. The images of SGC-7901 cells (a) with cccp (b, carbonylcyanide-m-chlorophenylhydrazone, positive control) and 3.13 (c), 6.25 (d), 12.5 μM (e) of **Ir-1** are shown in Fig. 5B. In the control, JC-1 emits red fluorescence. Treatment of SGC-7901 cells with cccp and different concentration of **Ir-1**, JC-1 emits green fluorescence. Moreover, the green fluorescent intensity increases with increasing the concentration of **Ir-1**. The changes from the red to green indicate that the complex can induce a decrease in the mitochondrial membrane potential. To further compare the effect induced by the different concentration of complex on the changes of MMP, the ration of red/green fluorescent intensity was determined by flow cytometry. In the control (Fig. 5C), the ratio of red/green fluorescence is 1.96, SGC-7901 cells were exposed to 3.13 and 6.25 μM of **Ir-1**, the ratios are 0.40 and 0.32, respectively. The decrease in the ratio of red/green fluorescence reveals that the red fluorescent intensity decreases and green fluorescent intensity enhances, which further demonstrates that **Ir-1** induces a decrease in the mitochondrial membrane potential in a concentration-dependent manner.

Reactive oxygen species levels assay

Many anti-proliferative drugs exhibit antitumor activity through the reactive oxygen species (ROS) accumulation in the process of apoptosis [41]. The level of ROS can be detected using DCHF-DA as fluorescent probe. DCHF-DA is a cell permeant dye and is cleaved by intracellular esterase into its non-fluorescent form (DCHF, 2′,7′-dichloro-3,6-fluorandiol). Then DCHF is oxidized by intracellular free radicals to produce a fluorescent product DCF (dichlorofluorescein) [42, 43]. As is shown in Fig. 6A, in the control, no obvious fluorescent spots are observed. After 24 h exposure of SGC-7901 cells to Rosup (b, positive control) and 3.13 (c), 6.25 (d), 12.5 (e) of **Ir-1**, bright fluorescent spots are found. Furthermore, more bright fluorescent spots are observed with increasing the concentration of **Ir-1**. The DCF fluorescent intensity was also detected by flow cytometry. In the control (Fig. 6B), the fluorescent intensity is 293. Treatment of SGC-7901 cells with 3.13 (b), 6.25 (c) and 12.5 μM (d) of **Ir-1** led to an increase of 1.30, 1.43 and 2.17 times than the original. Thus, the increasing

concentration induces an increase in the ROS levels. The data show that the complex can enhance the ROS levels.

Cell cycle arrest by flow cytometry

The apoptosis of tumor cells is often associated with genomic DNA damage and cell cycle perturbation [43, 44]. To estimate the effect of **Ir-1** on the cell cycle distribution, the cell cycle arrest was performed using flow cytometry. As shown in Fig. 7, in the control, the percentage in the cell at G0/G1 phase is 54.04%. After the treatment of SGC-7901 cells with 6.25 μM of **Ir-1**, the percentage in the cell at G0/G1 phase is 59.96%. An increase of 5.92% in the percentage of cells at G0/G1 phase was observed, accompanied by corresponding decrease in the percentage of cells in the S phases. The result suggests that the complex induces cell cycle arrest in SGC-7901 cell at G0/G1 phase.

Autophagy induced by Ir-1

It is well known that autophagy is a physiologically regulated process, under certain stress conditions, which allows degradation of the cytoplasmic contents including unfolded proteins and membranous organelles [45]. Recently, autophagy has become a burgeoning field in the therapy of various diseases and has been connected with the lethal mechanism of cancers [46, 47], which stimulates our strong attempt to explore whether **Ir-1** can trigger autophagy in SGC-7901 cells. To elucidate the effect of **Ir-1** on autophagy in SGC-7901 cells, the autophagy was investigated using MDC as fluorescent probe. It is well known that MDC fluorescent dye is a specific, in vivo marker for autophagic vacuoles [48], and MDC incorporation is an indicator of autophagic activity. As shown in Fig. 8A, surprisingly, the great autophagy flux activity of SGC-7901 cells was observed under fluorescence microscope, cells with typical feature of autophagy, autophagic vacuoles (AVs) are observed. The MDC fluorescent intensity was determined by flow cytometry (Fig. 8B), in the control (a), the fluorescent intensity of MDC is 2.92. SGC-7901 cells incubated with 3.13 (b), 6.25 (c) and 12.5 μM (d) of **Ir-1**, the MDC fluorescent intensity increases 20.1, 42.8 and 97.6 times than the original. The results indicate that the complex show a concentration-dependent manner to induce autophagy in SGC-7901 cells. In addition, the formation of autophagic vacuoles was further studied by assay of LC3 protein levels, which is often regarded as a marker of autophagy, and the conversion of LC3-I to LC3-II shows autophagy induction [49]. The amount of LC3-II is closely correlated with number of autophagosomers [50]. Seen from

Fig. 8C, a significant increase expression of LC3-II and Beclin-1 proteins was observed. This further confirms that the complex can induce autophagy in SGC-7901 cells. To investigate the effect of the autophagy on the cell viability, SGC-7901 cells were treated by different concentrations of the complex in the presence or absence of autophagic inhibitor 3-MA. As shown in Fig. 8D, compared with the control, the cell viability induced by **Ir-1** decreases in the presence of 3-MA, which suggests that the autophagy inhibits the cell death.

Fig. 9 **A** Microscope images of invading SGC-7901 cells (*a*) that have migrated through the Matrigel induced by 3.13 (*b*) and 6.25 μM (*c*) of **Ir-1** for 24 h. **B** Cell invasion assay result of **Ir-1** against SGC-7901 cell. *$P < 0.05$ represents significant differences compared with control. **C** The percentage of different concentration of the complex inhibiting cell invasion
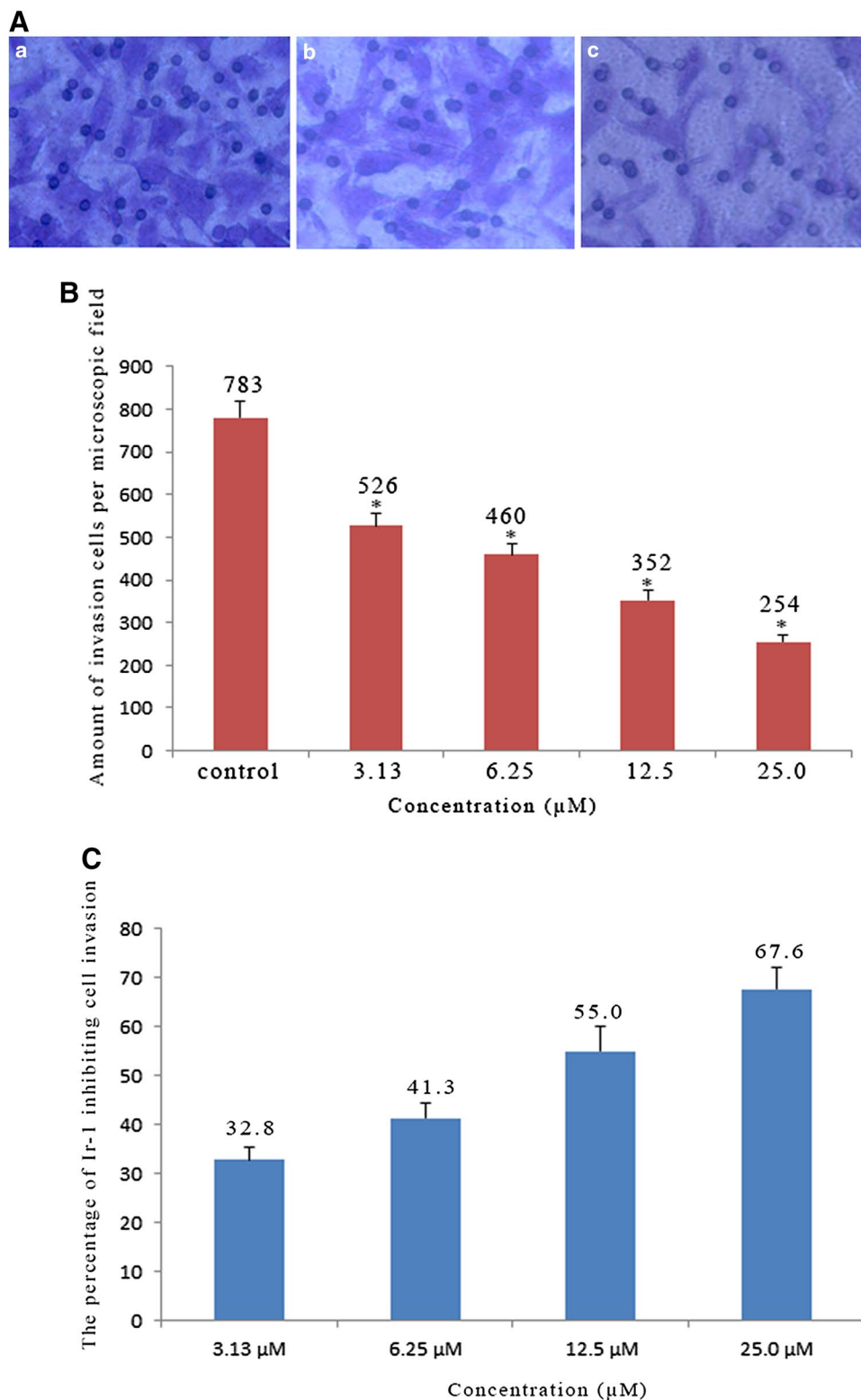
The cell invasion assay

It is interesting to investigate whether the **Ir-1** can inhibit invasion of SGC-7901 cells. The transwell invasion assay in SGC-7901 cells was treated by Matrigel invasion assay. The results obtained from the study were shown in Fig. 9A and B. SGC-7901 cells were exposed to 3.13, 6.25, 12.5 and 25.0 μM of **Ir-1**, the number of the invasion cells decrease gradually, and the percentages of **Ir-1** inhibiting cell invasion are calculated to be 32.8, 41.3, 55.0 and 67.6%, respectively. Therefore, complex **Ir-1** shows a concentration-dependent manner in the inhibiting cell invasion. These results demonstrate that the complex can effectively inhibit SGC-7901 cell invasion.

The expression of Bcl-2 family proteins by western blot

It is acknowledged that caspase-3 and -7 are pivotal activator of apoptosis as processing of their substrates result in morphological changes related with apoptosis, including membrane blebbing, chromatin condensation and DNA degradation 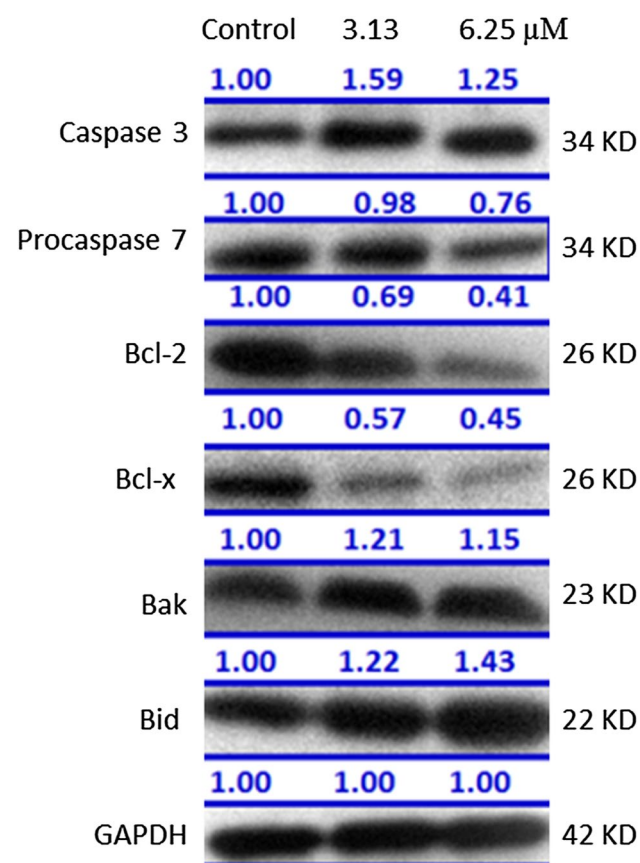[50]. Bcl-2 family proteins play important roles in the regulation of apoptosis though governing mitochondrial outer membrane permeabilization [51]. To clarify the mechanism of apoptosis induced by **Ir-1**, the expression levels of Bcl-2 family proteins were studied by western blotting analysis. After caspase 3, procaspase 7, Bcl-2, Bcl-x, Bak and Bid were incubated with different concentration of the complex (Fig. 10) for 24 h, the expression levels of caspase-3, bak and bid were significantly upregulated, whereas the levels of the anti-apoptotic proteins Bcl-2, Bcl-x and procaspase 7 were down-regulated. The results exhibit that the complex can regulate the expression of caspase 3, procaspase 7 and Bcl-2 family proteins.

Conclusions

A new ligand BTCP and its iridium complex $[Ir(ppy)_2(BTCP)PF_6$ (**Ir-1**) were synthesized and characterized. The complex shows high cytotoxic activity against the selected cell lines. In particular, **Ir-1** possesses very strong ability to kill SGC-7901 cell with a low IC_{50} value (3.9 ± 0.5 μM). The complex can induce autophagy and apoptosis and was uptaken with a concentration-dependent manner by SGC-7901 cell. In the assay of ROS and mitochondrial membrane potential, the complex increases the ROS levels and induces a decrease in the mitochondrial membrane potential. In addition, **Ir-1** inhibits the cell growth at G0/G1 phase. When the concentration of the complex is 25.0 μM, the percentage of the complex inhibiting cell invasion reaches 67.6%. The expression levels of caspase-3, bak and bid were upregulated, and the levels of the anti-apoptotic proteins Bcl-2, Bcl-x and procaspase 7 were down-regulated. In summary, the complex induces SGC-7901 apoptosis through a ROS-mediated mitochondrial dysfunction pathway, which was accompanied by the regulation of the expression of caspases and Bcl-2 family protein. The work is helpful for the design and synthesis of new Ir(III) complex as potent anticancer agents.

Fig. 10 The expression of Bcl-2 family proteins treated with 3.13 and 6.25 μM of **Ir-1** for 24 h

References

1. Aragon-Ching BJ, Dahut WL (2009) Update Cancer Ther 3:182–188
2. De Martel C, Ferlay J, Franceschi S (2012) Lancet Oncol 13:607–615

3. Kelland L (2007) Nat Rev Cancer 7:573–584
4. Harlos M, Ott I, Gust R, Alborzinia H, Wölfl S, Kromm A, Sheldrick WS (2008) J Med Chem 51:3924–3933
5. Boff B, Gaiddon C, Pfeffer M (2013) Inorg Chem 52:2705–2715
6. Haas KL, Franz KJ (2009) Chem Rev 109:4921–4960
7. Goswami TK, Chakravarthi BVSK, Roy M, Karande AA, Chakravarty AR (2011) Inorg Chem 50:8452–8464
8. Zhang C, Zeng CC, Lai SH, Xing DG, Li W, Han BJ, Liu YJ (2016) Polyhedron 106:115–124
9. Lai SH, Li W, Yao JH, Han BJ, Jiang GB, Zhang C, Liu YJ (2016) J Photochem Photobiol B Biol 158:39–48
10. Rijt SHV, Mukherjee A, Pizarro AM, Sadler PJ (2010) J Med Chem 53:840–849
11. Louie MW, Choi AWT, Liu HW, Chan BTN, Lo KK (2012) Organometallics 31:5844–5855
12. Liu Z, Habtemariam A, Pizarro AM, Fletcher SA, Kisova A, Vrana O, Salassa L, Bruijnincx PCA, Clarkson GJ, Brabec V, Sadler PJ (2011) J Med Chem 54:3011–3026
13. Liu Z, Salassa L, Habtemariam A, Pizarro AM, Clarkson GJ, Sadler PJ (2011) Inorg Chem 50:5777–5783
14. Huang HY, Yang L, Zhang PY, Qiu KQ, Huang JJ, Chen Y, Diao JJ, Liu JK, Ji LN, Long JG, Chao H (2016) Biomaterials 83:321–331
15. Wu ZZ, Mu JJ, Wang Q, Chen X, Jensen L, Yi CQ, Li MJ (2015) J Organomet Chem 791:175–182
16. Thangavel S, Paulpandi M, Friedrich HB, Murugan K, Kalva S, Skelton AA (2016) J Inorg Biochem 159:50–61
17. Almodares Z, Lucas SJ, Crossley BD, Basri AM, Pask CM, Hebden AJ, Phillips RM, McGowan PC (2014) Inorg Chem 53:727–736
18. Mukhopadhyay S, Gupta RK, Paitandi RP, Rana NK, Sharma G, Koch B, Rana LK, Hundal MS, Pandey DS (2015) Organometallics 34:4491–4506
19. Bach C, Willner H, Aubke F, Wang CQ, Rettig SJ, Trotter J (1996) Angew Chem Int Ed 35:1974–1976
20. Li Y, Tan CP, Zhang W, He L, Ji LN, Mao ZW (2015) Biomaterials 39:95–104
21. Amouri H, Moussa J, Renfrew AK, Dyson PJ, Rager MN, Chamoreau LM (2010) Angew Chem Int Ed 49:7530–7533
22. Xiong K, Chen Y, Yang CO, Guan RL, Ji LN, Chao H (2016) Biochimie 125:186–194
23. Li SPY, Lau CTS, Louie MW, Lam YW, Cheng SH, Lo KKW (2013) Biomaterials 34:7519–7532
24. Cao R, Jia JL, Ma XC, Zhou M, Fei H (2013) J Med Chem 56:3636–3644
25. Li GY, Lin Q, Sun LL, Feng CS, Zhang PY, Yu B, Chen Y, Wen Y, Wang H, Ji LN, Chao H (2015) Biomaterials 53:285–295
26. Chen Y, Xu WC, Zuo JR, Ji LN, Chao H (2015) J Mater Chem B 3:3306–3314
27. McBride HM, Neuspiel M, Wasiak S (2006) Curr Biol 16:R551–R560
28. Henze K, Martin W (2002) Nature 426:127–128
29. Paw W, Eisenberg R (1997) Inorg Chem 36:2287–2293
30. Sprouse S, King KA, Spellane PJ, Watts RJ (1984) J Am Chem Soc 106:6647–6653
31. Mosmann T (1983) J Immunol Methods 65:55–63
32. Lo KK, Lee TK, Lau JS, Poon WL, Cheng SH (2008) Inorg Chem 47:200–208
33. He L, Liao SY, Tan CP, Lu YY, Xu CX, Ji LN, Mao ZW (2014) Chem Commun 50:5611–5614
34. Li SPY, Lau CTS, Louie MW, Lam YW, Cheng SH, Lo KKW (2013) Biomaterials 34:7519–7532
35. Hickman JA (1992) Cancer Metastasis Rev 11:121–139
36. Li W, Nie S, Yu Q, Xie M (2009) J Agr Chem 57:6685–6691
37. Li GY, Du KJ, Wang JQ, Liang JW, Kou JF, Hou XJ, Ji LN, Chao H (2013) J Inorg Biochem 119:43–53
38. Alapetite C, Wachter T, Sage E, Moustacchi E (1996) Int J Radiat Biol 69:359–369
39. Leung CW, Hong Y, Chen S, Zhao E, Lam JW, Tang BZ (2013) J Am Soc Chem 135:63–65
40. Liu SH, Zhao JH, Deng KK, Wu Y, Zhu JW, Liu QH, Xua HH, Wu HF, Li XY, Wang JW, Guo QF (2015) Spectrochim Acta A 140:202–209
41. Trachootham D, Alexandre J, Huang P (2009) Nat Rev Drug Discov 8:579–591
42. Wrona M, Patel K, Wardman P (2005) Free Radic Biol Med 38:262–270
43. Shapiro GI, Harper JW (1999) J Clin Invest 104:1645–1653
44. Wang D, Lippard SJ (2005) Nat Rev Drug Discov 4:307–320
45. He CC, Klionsky DJ (2009) Annu Rev Genet 43:67–93
46. Shintani T, Klionsky DJ (2004) Science 306:990–995
47. Kondo Y, Kanzawa T, Sawaya R, Kondo S (2005) Nat Rev Cancer 5:726–734
48. Harikumar KB, Kunnumakkara AB, Sethi G, Diagaradjane P, Anand P, Pandey MK, Gelovani J, Krishnan S, Guha S, Aggarwal BB (2010) Int J Cancer 127:257–268
49. Kabeya Y, Mizushima N, Ueno T, Yamamoto A, Kirisako T, Noda T, Kominami E, Ohsumi Y, Yoshimori T (2000) EMBO J 19:5720–5728
50. Danial NN, Korsmeyer SJ (2004) Cell 116:205–219
51. Chambers AF, Groom AC, MacDonald IC (2002) Nat Rev Cancer 2:563–572